



Investigation the Synthesis of Nano-SAPO-34 Catalyst Prepared by Different Templates for MTO Process

Haiyan Liu¹ · Ehsan Kianfar^{2,3}

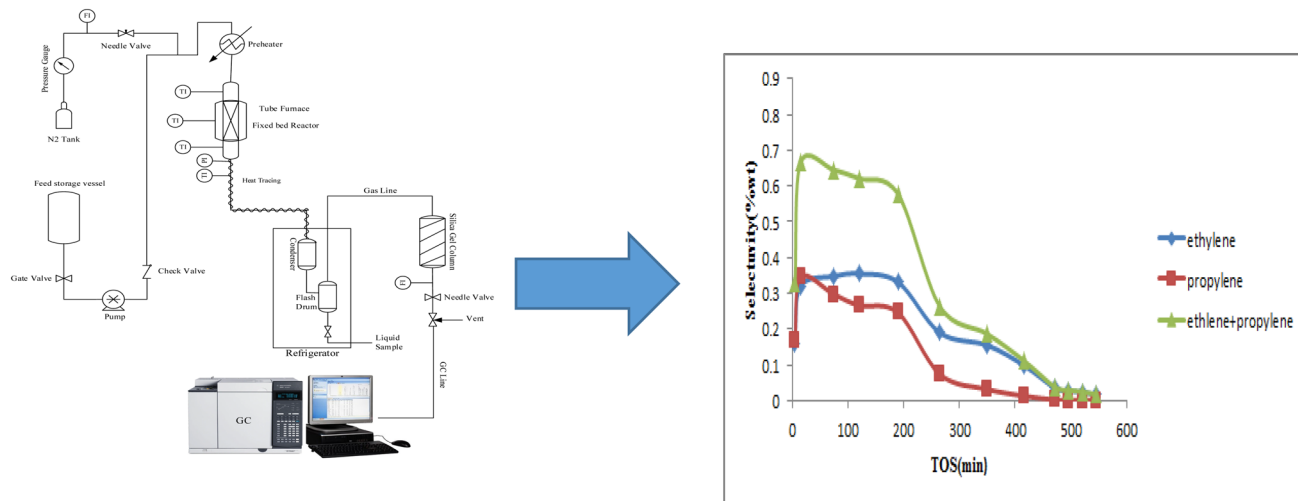
Received: 27 April 2020 / Accepted: 26 July 2020 / Published online: 6 August 2020
© Springer Science+Business Media, LLC, part of Springer Nature 2020

Abstract

In this paper, nine samples of SAPO-34 Nanocatalysts were synthesized, at three temperatures (170, 190, 210 °C) and three times (12, 24, and 36 h) using the hydrothermal treatment and experimental design approach. All samples were characterized by XRD, SEM, FTIR, BET, and NH₃-TPD techniques, to evaluate the morphology, crystal size, and surface acidity. The catalytic performance of SAPO-34 zeolites for methanol to light olefins (MTO) was investigated in a fixed-bed reactor at 410 °C. According to catalytic results, all prepared catalysts showed similar trends, but olefin selectivity and lifetime were greatly different. Catalysts synthesized at 170 °C and 24 h because of their high crystallinity, the small size of crystals and high surface area showed relatively high ethylene and propylene selectivity of 48.71% and 32.6%, respectively. Sample with low crystallinity, synthesized at 210 °C, and 36 h because of the existing high value of the SAPO-5 and amorphous phase, deactivate rapidly. Comparing with the other sample, the sample synthesized at 170 °C and 12 h because of high crystallinity, mild acidity, and small crystal size possesses a longer lifetime.

Graphic Abstract

Hierarchical nine samples of SAPO-34 Nano catalysts were synthesized, at three temperatures (170, 190, 210 °C) and three times (12, 24 and 36 h.) using hydrothermal treatment and experimental design approach. Comparing with the other sample, the sample synthesized at 170 °C and 12 h. because of high crystallinity, mild acidity and small crystal size, possesses a longer lifetime.



Keywords SAPO-34 · MTO process · Crystallinity · Selectivity · Light olefins

1 Introduction

Light olefins such as ethylene, propylene, and butylene are mainly used in the petrochemical industry. Due to the increasing demand for light olefins in the industry and the future shortage of petroleum resources, the process of converting methanol to olefins (MTO) using non-oil sources has been considered as an alternative. Coal and natural gas are abundant in nature and the methods of converting them to methanol are well known today [1–3]. Coal gasification or steam reforming of natural gas to produce synthetic gas (CO and hydrogen gas) can lead to methanol production. Methanol can also be catalytically converted to gasoline or olefins depending on the effective process and catalyst factors used [4, 5]. Due to the use of crude methanol in the MTO unit and because the feed does not require primary distillation, if the MTO unit is installed alongside the methanol unit, its capital costs will be reduced [6–10]. The use of methanol can have advantages such as easier and less expensive transportation than ethane [10–14, 84–87]. Among the available catalysts, SAPO-34 is the most suitable catalyst for this process due to its small cavities and medium acidity. One of the main problems of MTO units is the rapid deactivation of SAPO-34, which can also be affected by the synthesis factors, so it is possible to optimize the catalyst performance by modifying the synthesis conditions [15–17, 88–90]. The synthesis gas is converted to olefins, isoparaffins, gasoline products, and aromatics after conversion to methanol using Fischer Tropsch reaction (FTS) and acid catalysts [18–21, 91–93]. This process has advantages over thermal breakdown with steam, naphtha, and light petroleum cuttings because it provides a wider and more flexible range for the ethylene to propylene ratio [22, 23, 94–97]. Other advantages include the production of limited byproducts compared to other fracturing methods resulting in simpler recycling and purification systems, simpler unit use than conventional units due to low paraffin content do and no need for propane/propylene and ethane separator systems [24–27]. Ethylene is another characteristic of the process due to the production of propylene and ethylene with a purity of more than 98% [28–30]. Of course, there are other methods such as oxidative methane coupling (OCM), oxidative dehydrogenation of kinds of paraffin, and internal conversion of olefins that are not currently commercially used [31–33, 79, 80]. The aim of this article, Studies on the effect of temperature and crystallization time on SAPO-34 catalysts show that most of the activities involved are related to the effect of this parameter on the morphology and physical, chemical, and catalytic properties of the catalyst and in none of the catalyst performance. It has not been examined in the MTO process [34, 35, 81–83]. The aim of this

research investigates the simultaneous effect of crystallization temperature and time as influencing variables on the structural and acidic properties of SAPO-34 catalyst, Optimizes the performance of the catalyst to produce light olefins in the MTO process.

Izadbakhsh et al. [36], Prepared SAPO-34 catalyst with different Si/Al ratios (0.5–0.5) at crystallization temperature of 215–190 °C by hydrothermal method and obtained samples by various XRD, SEM/EDX experiments NH₃-TPD, FTIR, and nitrogen uptake were investigated. EDX data showed that increasing the Si/Al ratio in the initial gel blend increased the silicon content in the product. According to XRD and SEM results, the crystallinity of the samples increased with increasing Si/Al ratio. Of course, the relative increase in the ratio of silicon to aluminum did not only increase the crystallinity but also decreased it. The results obtained in the study of the catalyst performance in the reactor with reaction temperature of 400 °C and methanol discharge WHSV = 1 h⁻¹ showed that the SAPO-34 crystallinity affected by the change of Si/Al ratio is an important factor in the coke production of methanol to coke process. It is olefins. High crystallinity samples (Si/Al=0.13–0.22) lead to longer catalyst life in the reactor of 3 h, which is longer than the life of the less crystalline samples (1 h).

Shen et al. [37] investigated the effect of Si on the acidic properties of SAPO-34 using solid-state NMR analysis. The results showed that there are two types of Bronsted acidic sites in SAPO-34, one of which is stronger than the acidic site in ZSM-5. Si species and their distribution in the composition structure depend on the Si content. Si islands are mostly formed when the Si content is high, while the low Si content only generates 4 Si (OAL) species. Si has little effect on the strength of the SAPO-34 Bronsted Acids but can alter the catalyst acidity.

Wilson et al. [27] investigated the effective properties of SAPO catalysts on reactor performance such as shape selectivity, acidic site strength, acidic site content, crystal size, and Si content in the catalyst. Evaluation of small completely molecular sieve in the MTO process shows that SAPO-34 due to its high selectivity to C₂-C₃ olefins, low production of paraffin and aromatic byproducts, and favorable conditions for catalyst recovery compared to other catalyst species. SAPO performs best. Decreasing the amount of Si results in reduced olefin production and increased catalyst life. There is also no direct relationship between the amount of Si in the composition and the number of acidic sites, although in low Si there is usually an acidic site per Si in the structure.

Wang et al. [38] investigated the effect of silicon on the Cu/SAPO-34 and HSAPO-34 catalyst properties. In the three ratios tested for Si/Al in the experiments, it was found that the sample had the smallest crystal size with a Si/Al ratio of 0.3. The TPD experiment showed that the sample

had the highest amount of silicon at the Si/Al=0.85 ratios. As for the Cu/SAPO-34 catalyst, studies showed that the number of acidic sites increased with increasing Si content in the samples. The EPR and H₂-TPR results showed that the Si and Al values affect the number of individual Cu²⁺ ions in the catalyst.

Izadbakhsh et al. [39] produced a low-silicon SAPO-34 catalyst by hydrothermal method. The examination of the samples showed that the total acidity in the samples with low silicon was much lower than the samples with higher silicon. Bronsted acid sites remained almost constant after a threshold value for silicon, with changes below these threshold values reported.

2 Experiment

2.1 SAPO-34 Catalyst Preparation

Based on the investigations that have been performed on the gel composition of SAPO-34 and mentioned in the introduction of the present article, the final gel composition was selected to be 1 Al₂O₃:1 P₂O₅: 0.4 SiO₂: 1TEAOH: 0.5 MOR: 0.5 TEA: 70 H₂O. Aluminum, phosphorous and silica sources were aluminum isopropoxide, phosphoric acid 85% wt. in water and silica sol 40% wt. in water, respectively. For the synthesis of SAPO-34, different methods have been reported in the literature. The point is that the order of adding the raw materials is a key factor, and if the template changes the previous sequence of addition may not be applicable. Prepared gel was aged at 50 °C for 24 h and placed in 120 cc Teflon lined stainless steel under auto-genius pressure at 200 °C for 24 h under hydrothermal synthesis. Then, the solid product was collected by centrifugation and then washed three times with deionized water. Drying was performed at 110 °C overnight and calcination was accomplished at 550 °C for 6 h with a temperature ramp of 1 °C/min [40–44]. Table 1 shows Different crystallization times and temperatures for the preparation of SAPO-34 catalysts.

2.2 Reactor Test

Figure 1 is an overview of the laboratory unit. After the catalyst restoration, a mixture containing methanol and water (30% by weight methanol solution, 99.9%, Merck) is pumped into the furnace. The feed then enters the reactor from the bottom of the furnace. After the reaction, the outflow from the reactor enters the condenser and lowers the temperature to prevent secondary reactions. At this point, water and heavy hydrocarbons become liquid and accumulate in the condenser. The residual gas stream is transferred to the GC for analysis or to the outside environment. In addition to the feed stream of methanol and water entering the reactor, there

Table 1 Different crystallization times and temperatures for the preparation of SAPO-34 catalysts

Sample	Temperature(°C)	Time(hr)
SAPO-34(S ₁)	170.0	12
SAPO-34(S ₂)	170.0	24
SAPO-34(S ₃)	170.0	36
SAPO-34(S ₄)	190.0	12
SAPO-34(S ₅)	190.0	24
SAPO-34(S ₆)	190.0	36
SAPO-34(S ₇)	210.0	12
SAPO-34(S ₈)	210.0	24
SAPO-34(S ₉)	210.0	36

is another stream that is attached to the nitrogen gas capsule. Because of the time gap between the synthesis and the reactor test, nitrogen gas was used to dehydrate and restore the catalysts. This step was performed before the reaction at 550 °C with a flow rate of approximately 40 ml/min for one hour [45–49]. To adjust the current intensity before injection of one Flow meter bubble was used. The furnace used in this laboratory unit, which is used to supply the heat required for the reactor and to perform the MTO reaction, is a pipe furnace manufactured by Azar Furnace Company. The furnace has a length of 45 cm and an inner diameter of 4.5 cm. GC unit used in a laboratory unit, Hewlett-Packard 5890 Flame Ionization Detector (FID), equipped with Agilent J&W GS-alumina column measuring 30 μm* 0.53* mm 30 m, manufactured by Hewlett-Packard and for the detection of hydrocarbon compounds Is. In this system, it is not possible to measure and detect hydrogen, carbon dioxide, and carbon monoxide, so the weight percent of these three compounds in the gas sample is calculated by the elemental mass balance of the identified gases [50–52].

3 Results and Discussion

3.1 Investigation of Structural Properties of Catalysts

Structural and acidic properties of the catalysts prepared on some samples were analyzed by XRD, SEM, FTIR, BET, and NH₃-TPD.

3.1.1 Crystallinity Study of Catalysts

Figure 2 X-ray diffraction (XRD) images to determine the crystalline phase, Phase purity and crystallinity are the catalysts synthesized By comparing the obtained patterns and the reference patterns, we conclude all samples had SAPO-34 related peaks ($2\theta \approx 9.66^\circ, 13^\circ, 16, 17.9^\circ,$

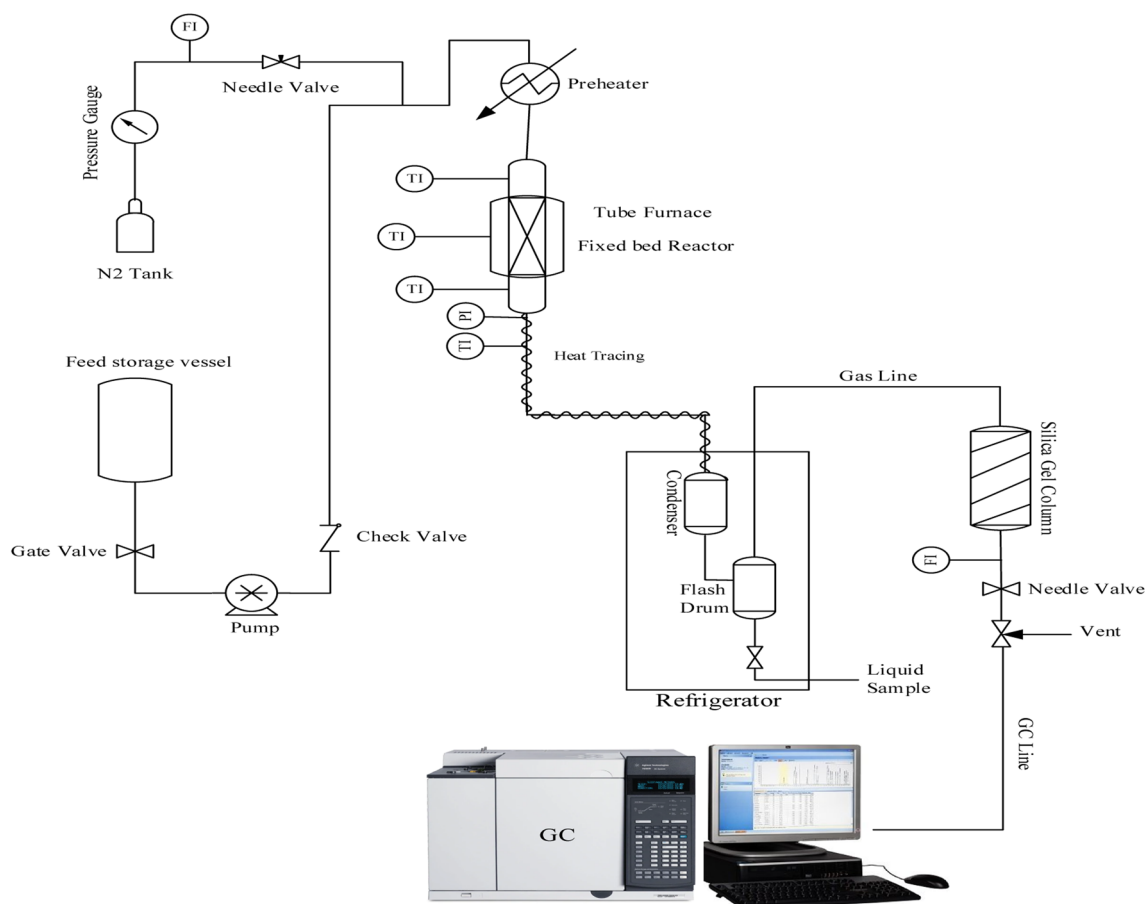


Fig. 1 Laboratory process for performing the MTO process

Table 2 Relative crystallinity of catalysts prepared

Sample	Relative Crystallinity (%)	Crystal Size (μm)
SAPO-34(S ₁)	71.64	1.52
SAPO-34(S ₂)	74.44	1.61
SAPO-34(S ₃)	68.08	1.96
SAPO-34(S ₄)	65.00	1.74
SAPO-34(S ₅)	55.00	1.90
SAPO-34(S ₆)	54.89	1.81
SAPO-34(S ₇)	63.51	1.51
SAPO-34(S ₈)	54.06	1.63
SAPO-34(S ₉)	53	1.80

20.52°, 25°, 25.9°, 30.8°, 31.1°) [53–55]. According to XRD diagrams, the S₆ and S₈ and S₉ samples have a peak at $2\theta \approx 7.5^\circ$, which can be attributed to SAPO-5 zeolites [56–58]. Table 2 percent crystallinity of each sample was reported. An XRD spectrum peak of crystalline and amorphous is set and, the percentage of crystallinity obtained from X-ray measurements is determined by the ratio of the

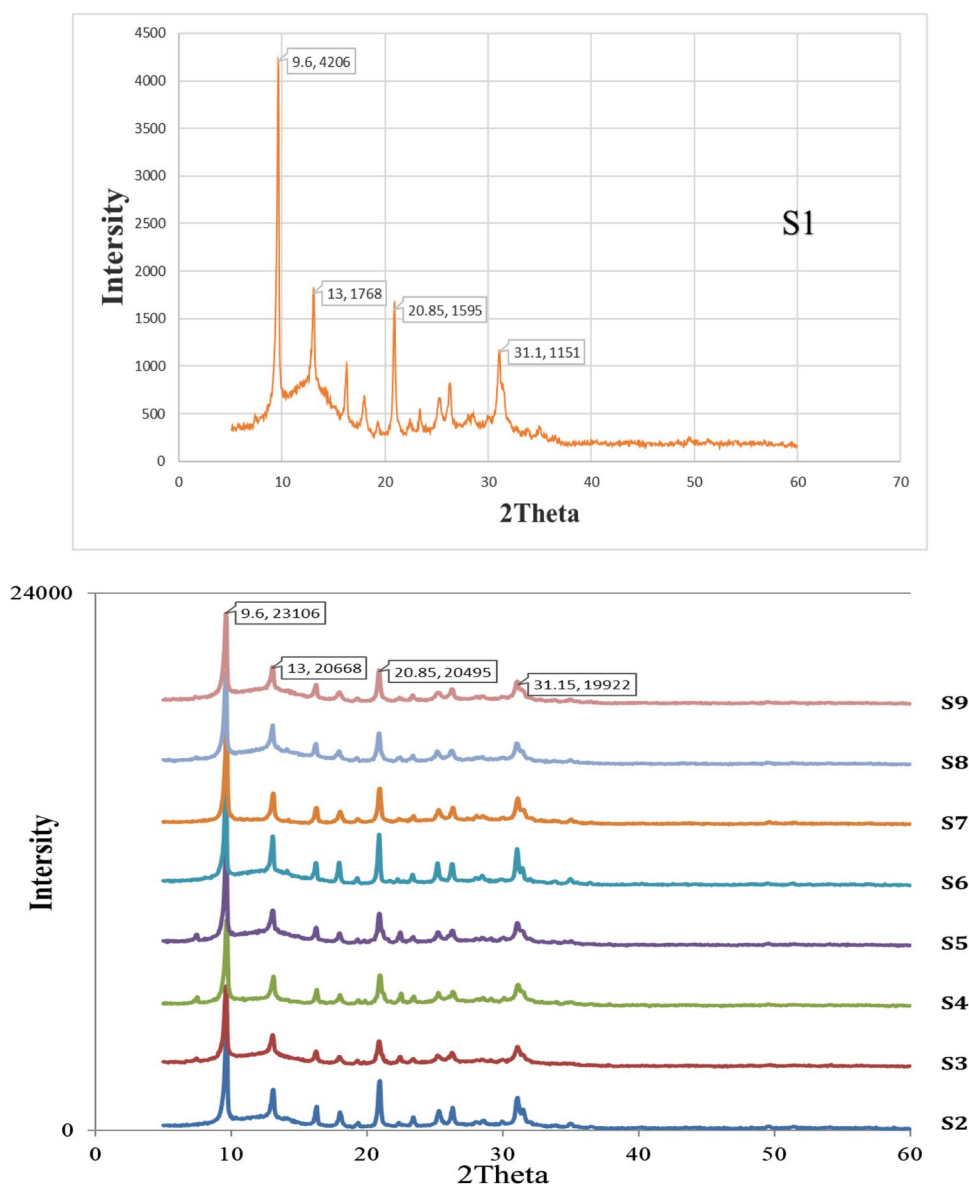
crystalline peak intensities to the sum of the crystalline and amorphous intensities [59].

The crystallite sizes of samples that are reported in Table 2 were determined based on the Scherrer's equation (Eq. 1). In this equation, D is crystallite size (nm), λ is X-ray wavelength approximately equal to 1.541 Å, β is the line width at half the maximum intensity (FWHM), and θ is bragg angle. Indeed, to determine the crystallite size of catalysts, the XRD diffraction patterns is used and the Highscore plus software is capable to calculate this parameter.

$$D = \frac{0.9\lambda}{\beta \cos\theta} \quad (1)$$

Quantitative study of FESEM images was done by Image J software and the range of particle sizes that are determined by FESEM analysis is reported in Table 2. It is true that particle size is obtained by FESEM analysis. Figure 3 illustrates the relative crystallinity and the crystallite size calculated with the Eq. (1) (considering intense peak at $2\theta = 9.5^\circ$, 13° , and 20.5°) and Eq. (2), respectively. It is

Fig. 2 XRD pattern for prepared catalyst



worth mentioning that the nonmodified SAPO-34 with the maximum crystallinity was considered as the reference.

$$\text{Relative crystallinity (\%)} = \frac{I_{\text{Crystalline}}}{I_{\text{Crystalline}} + I_{\text{Amorphous}}} \times 100 \quad (2)$$

The data in Table 2 show that except for S1, S2 and S3, the samples synthesized at constant crystallization temperature increased with crystallization time and also the samples synthesized at constant crystallization time, with increasing crystallization temperature. The percentage of crystallinity decreased and for the samples synthesized at constant crystallization time, with increasing crystallization temperature, crystallinity Dropped. According to the peak indexes of S1, S2, and S3 samples (samples synthesized at a

crystallization temperature of 170 °C at three times 12, 24, and 36 h), firstly, with increasing crystallization time crystallinity increased and then peak intensity decreased. Further increasing of hydrothermal time can enhance the formation of the amorphous phases.

The crystallinity percentage of S7, S8, and S9 samples (samples synthesized at 210 °C and crystallization time of 12, 24, and 36 h) with peaks obtained from XRD analysis indicated this. That there are impurities in sample S8 and little in sample S9 and the peaks of $2\theta = 7.5, 22.5$ prove this fact. And despite the increase in SAPO-34 index peaks in sample S9 compared to sample S7, the presence of intrusive peaks in the sample S8 reduced the crystallinity, and in the sample, S9 although the gross phase decreased compared to the sample S8. The peak intensities of the pure phase index decreased and resulted

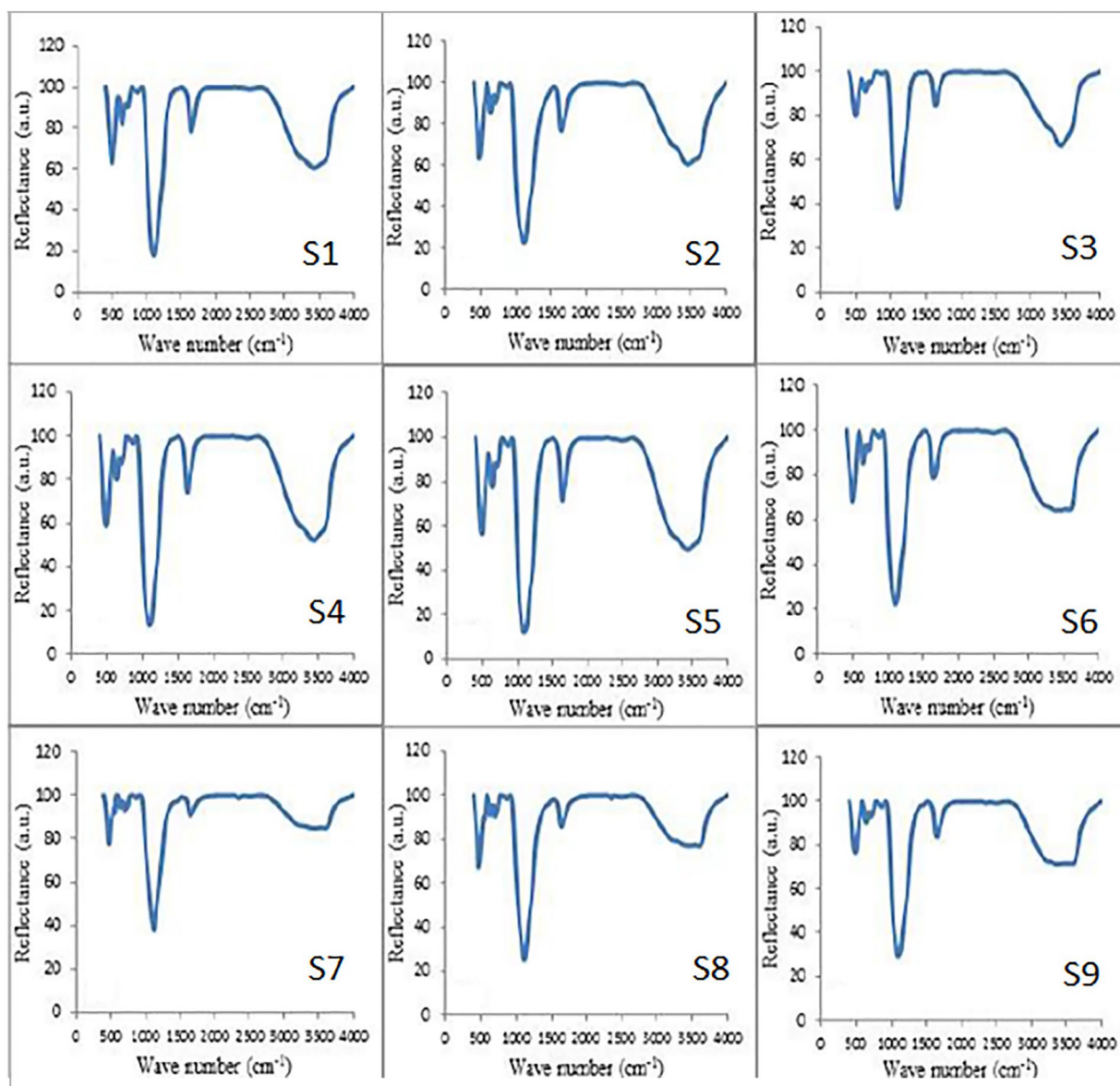


Fig. 3 FTIR pattern for prepared catalysts

in a decrease in crystallinity at a temperature of 210 °C. compared to sample S8, for S9. Despite the decrease in the gross phase content, the peak intensities of the pure phase index decreased and caused a decrease in crystallinity at a temperature of 210 °C. The trend of crystallinity decreasing at constant time and different temperatures is also due to the possible instability of SAPO-34 and its conversion to amorphous phases and other impurities. For example, at a constant time of 36 h with increasing crystallization temperature, presence of impurity peaks,

in the angles, $2\theta = 7.5, 19.9, 22.5$ this has led to a decreasing trend [60–62].

3.1.2 FT-IR Analysis

The results of the FTIR analysis to specify functional groups and bonds formed in the catalyst structure are shown in Fig. 3. SAPO-34. Catalyst has specific peaks at $621\text{--}626\text{ cm}^{-1}$, $484\text{--}480\text{ cm}^{-1}$, $713\text{--}877\text{ cm}^{-1}$, and $1093\text{--}1402\text{ cm}^{-1}$ related to TO Bands in Six-membered Rings, Silicon Quadrilateral TO Bands and symmetric

and asymmetric vibrations of TOT, respectively. Also, the hydroxyl group bonds that play a major role in the catalyst performance are index links in the SAPO-34 catalyst. The FTIR spectra of the samples in the OH bond range have five peaks in the wavelengths of 3413, 3475, 3554, 3720, and 3739 cm^{-1} . The last three peaks are related to the POH, SiOH, AlOH bonds, respectively. The other two peaks in the range of 3413–3477 cm^{-1} belong to Si–OH–Al bonds and are attributed to the outermost acidic sites. The intensity of this peak, which is Si–OH–Al bond strength, correlates to the number of acidic sites [63–67]. By comparing the intensity of this peak for the three samples S5, S2, and S8 (synthesized at 24 h and Temperature 170, 190, 210 $^{\circ}\text{C}$), shows that acidic strength is in order of $\text{S2} > \text{S8} > \text{S5}$, which is confirmed by TPD analysis.

3.1.3 SEM Analysis

SEM was used to study the morphology shape and size of the synthesized crystals. Figure 4 shows the images of the SEM for nine synthesized samples. The SEM images of the samples show that the morphology of all the samples as expected for SAPO-34 is cubic and the dominant phase in all samples is SAPO-34. S8, S6, and S9 samples in addition to cubic particles have hexagonal geometrical objects that belong to SAPO-5 [52, 67, 68]. However, due to the low SAPO-5 catalyst in the sample S9, the particles of this impurity are not visible in the SEM analysis.

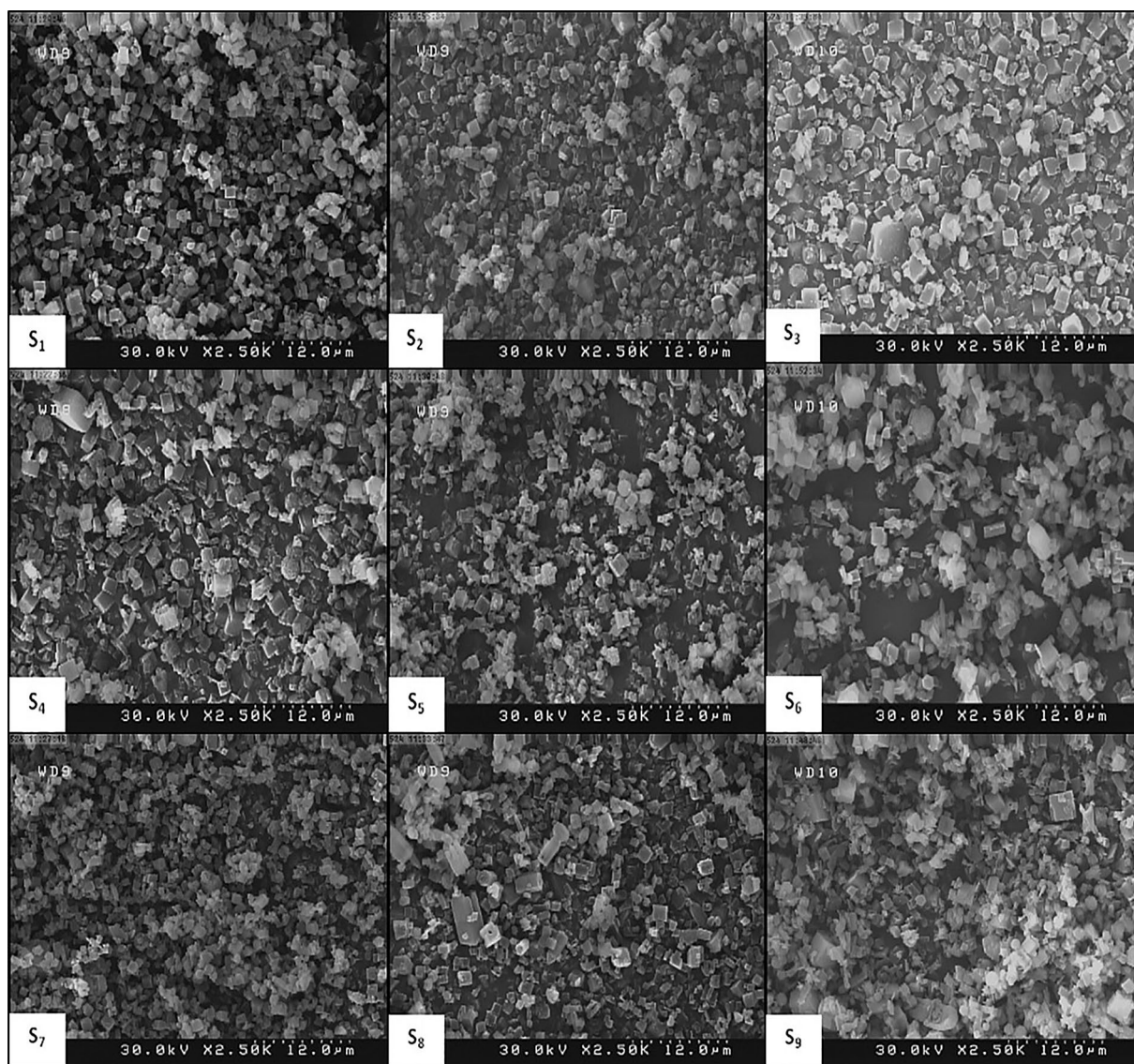


Fig. 4 SEM pattern for prepared catalysts

3.1.4 BET Analysis

The specific surface area of the catalyst is also very important in its catalytic activity. BET analysis was used to measure the surface area of the synthesized samples. Five synthesized samples with suitable particle size and high crystallinity were selected to investigate the effect of temperature and crystallization time on the specific surface area. The results of the BET analysis to determine the surface area, size, and volume of the catalyst holes are presented in Table 3. As shown, all samples have a relatively high specific surface area. Also, the results show that as the temperature and time of crystallization change the size of the holes, their volume and surface area change, which can affect the selectivity and yield of light olefins. For example, comparing two S2 and S5 samples, both synthesized at 24 h, shows with increasing the synthesis temperature from 170 to 190 °C, the surface area and pore volume decrease from 527.24 to 403.58 m²/g and from 0.292 to 0.246 cm³/g, respectively. Compared to other samples, the S6 catalyst has the highest surface area and pore volume, due to the smallest crystal size and the highest intracellular porosity [59].

Also according to the SEM image of sample S6, the sample contains an almost uniform distribution of large and small crystals and on the one hand, small crystals supplying more outer surface area and large crystals supplying more inner surface area, therefore, the special surface area which is total It is of internal and external surface area, for this sample more than other samples. Also according to Table 3, sample S6 (sample synthesized at a crystallization temperature of 190 °C for 36 h) has the lowest area (330/891 m²/g), due to the lowest crystallinity percentage (54.6) among the samples. S2, S4, S5, S6, and S8 and the large crystal size (1.816 μm), respectively.

Table 3 BET for prepared catalyst

Sample	Surface area (m ² /g)	Pore volume (cm ³ /g)	Pore size (°A)
SAPO-34(S ₂)	527.24	0.29	22.13
SAPO-34(S ₄)	462.83	0.26	23.19
SAPO-34(S ₅)	403.58	0.24	24.40
SAPO-34(S ₆)	330.89	0.21	25.92
SAPO-34(S ₈)	467.70	0.26	22.18

3.1.5 Temperature Programmed Desorption (TPD) Analysis

The temperature-programmed desorption of ammonia (NH₃-TPD) analysis to investigate the acidic properties and catalytic behavior and distinguish of acid strength and the amounts of acid sites of three samples of S₂, S₅ and S₈ are shown in Fig. 5 and Table 4. These samples were selected for NH₃-TPD analysis to provide comparative conditions for the study of time and temperature changes. As previously reported, the NH₃-TPD profiles of SAPO-34 catalysts showed two maxima appeared at about 200 and 400 °C, corresponding to weak and strong acid sites, respectively [69]. The first peak in the NH₃-TPD diagrams is generally related to the weak acidic sites, caused by TOH bonds (T can be Al, Si, or P). It is at the center of four-dimensional structures that are only capable of converting methanol to dimethyl ether and are not capable of converting dimethyl ether to light olefins. The large area under this peak is due to the presence of incomplete structures in the catalyst composition resulting in reduced sample crystallinity [70, 71]. Among these three catalysts, the S8 sample, synthesized at 210 °C and 24 h, with relatively lower crystallinity (0.554) have the highest weak acid sites as shown from the first peak in NH₃-TPD profile. The second peak in the NH₃-TPD diagram shows

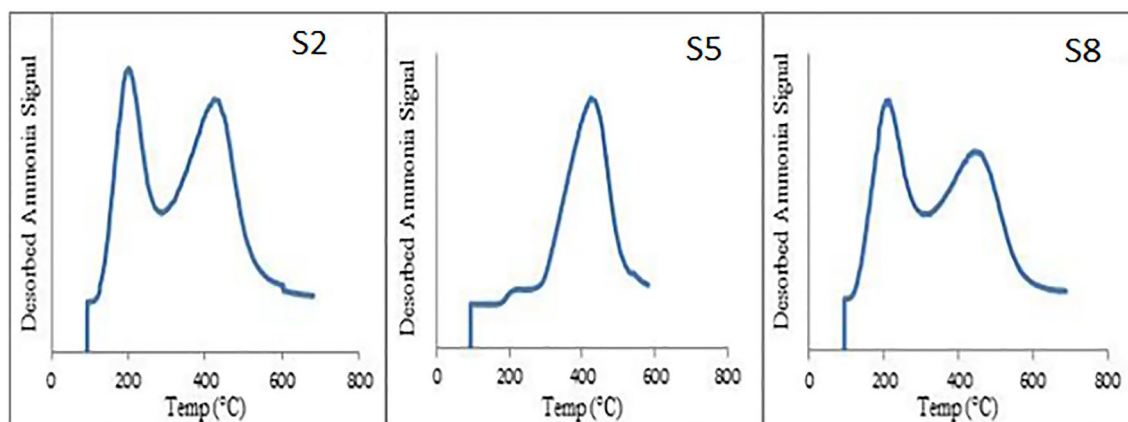


Fig. 5 NH₃-TPD patterns of S₂, S₅, and S₈ catalysts

the strong acidic sites caused by the hydroxyl groups -SiOHAl- in the catalyst. The strong absorption peaks at high temperatures are due to a large number of strong acid sites and Si (0-3Al) species or more silicon islands in the catalyst [72–74]. These sites are suitable for the production of light olefins. The higher this peak appears at the higher the strength of these acidic sites in the sample [75–78]. For the sample S₂, the second peak appeared at a higher temperature (434 °C) than other catalysts, so this sample has the highest strength of the strong acidic sites. On the other hand, the intensity of the second peak indicates the number of acidic sites and is proportional to the amount of ammonia excreted, which is higher for the sample S₂ than for the other two samples. As it is shown in Table 4, S₂ and S₈ samples have most acidic sites and

the total amount of desorbed NH₃ for them was 2.584 and 2.708 mmol/g, respectively.

3.1.6 Catalyst Performance

The MTO process was performed on each catalyst in the methanol-to-olefin reaction at several consecutive times. For the nine catalysts, the diagrams of ethylene and propylene selectivity changes over time on stream are shown in Figs. 6, 7, 8, 9, 10, 11, 12, 13, 14. In general, all the diagrams (except for the sample S₈) generally show three stages, especially for the sum of the olefins produced. The first stage is the time it takes to reach selectivity from its initial value to the maximum value attributed to Induction Time. This time lag can be due to the low concentration of

Table 4 NH₃-TPD analysis for prepared catalysts

Catalyst name	Acidity distribution (mmol NH ₃ /g catalyst)			Desorption temperature(°C)	
	Weak(A*)	Strong(C)	Total acidity	First peak	Second peak
S ₂	0.99	1.58	2.58	201	423
S ₅	0.06	1.51	1.57	215	425
S ₈	1.22	1.48	2.70	208	453

Fig. 6 Catalyst S1 reactor performance (synthesized at 170 °C for 12 h)

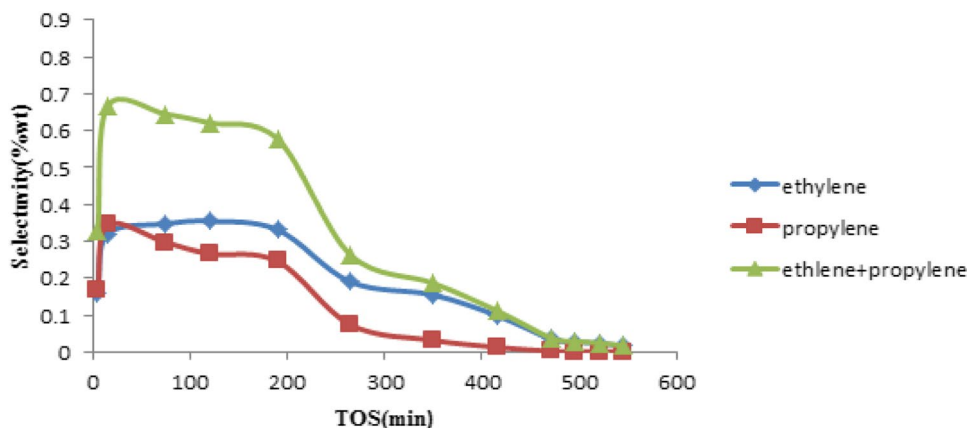


Fig. 7 Catalyst S2 reactor performance (synthesized at 170 °C for 24 h)

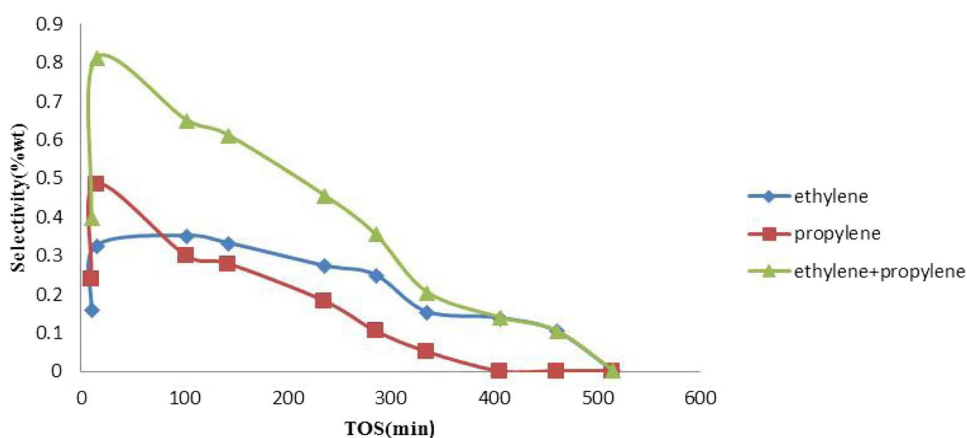


Fig. 8 Catalyst S3 reactor performance (synthesized at 170 °C for 36 h)

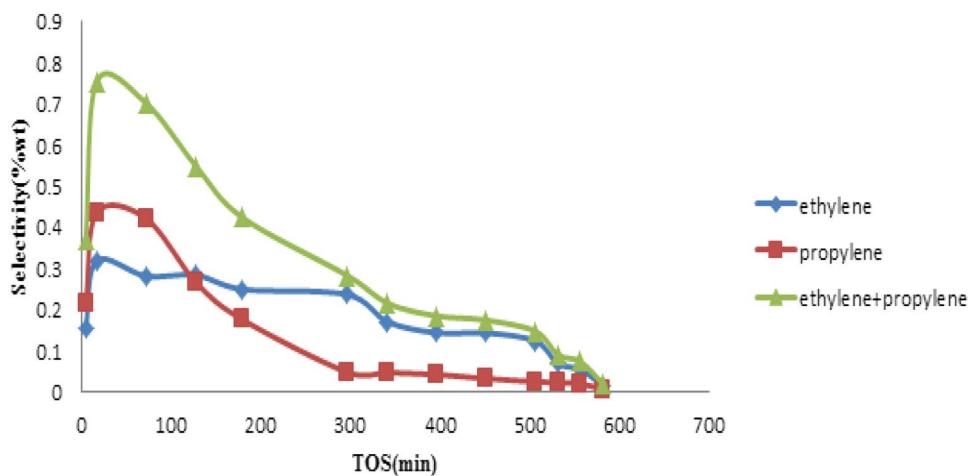


Fig. 9 Catalyst S4 reactor performance (synthesized at 190 °C for 12 h)

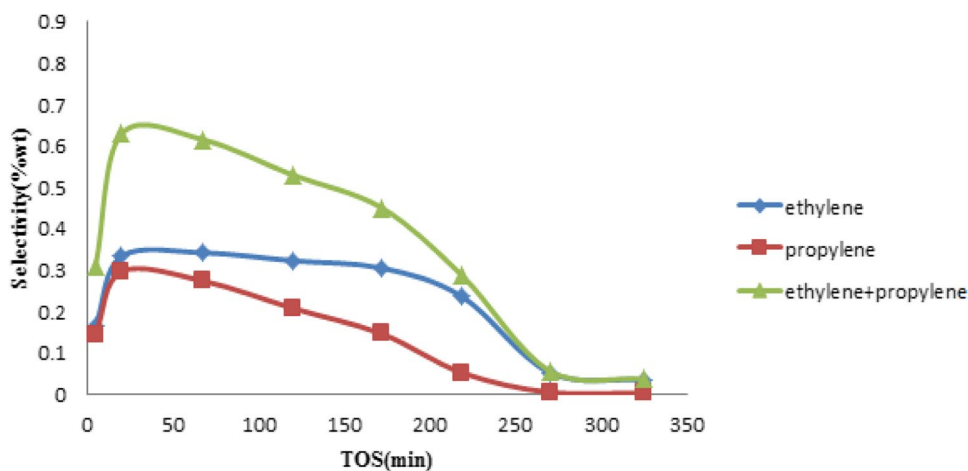
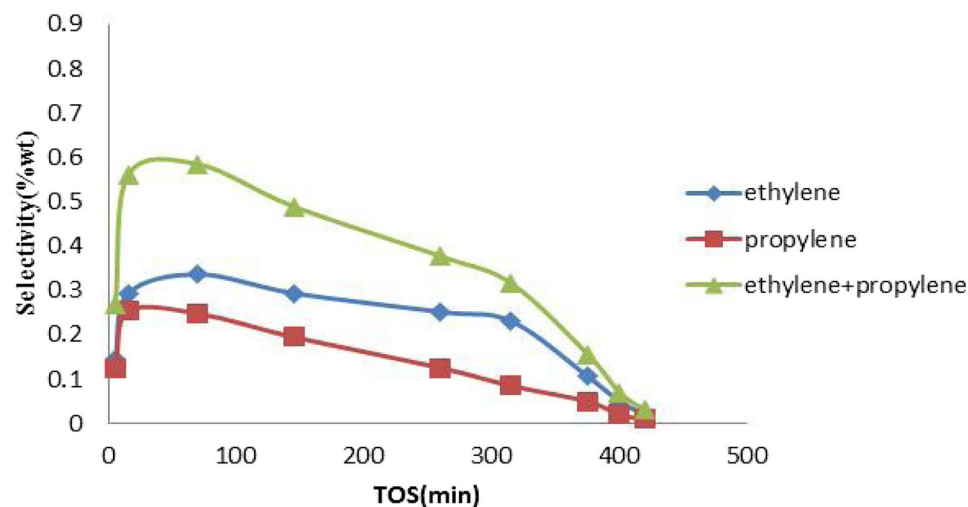


Fig. 10 Catalyst S5 reactor performance (synthesized at 190 °C for 24 h)



methanol in the feed, which requires a period for the reactant to enter the acidic active sites and produce products through the intermediates [36]. of course, the size of the crystals and their External surface area can also affect the ease of

access of catalysts to active sites [59] and vary from sample to sample, for example, in S2 sample (synthesized at 190 °C for 24 h) with smaller crystals (1.615 μm) and larger surface area (275.25 m^2/g) and consequence with shorter induction

Fig. 11 Catalyst S6 reactor performance (synthesized at 190 °C for 36 h)

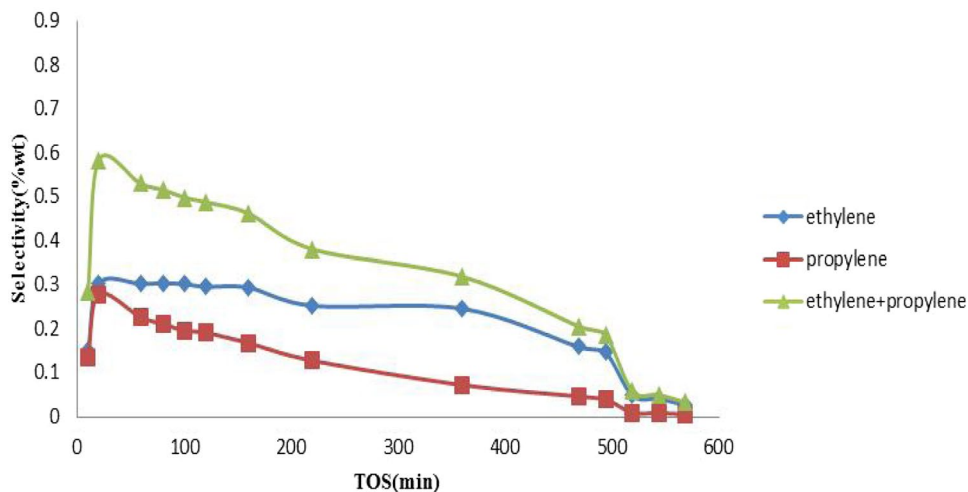


Fig. 12 Catalyst S7 reactor performance (synthesized at 210 °C for 12 h)

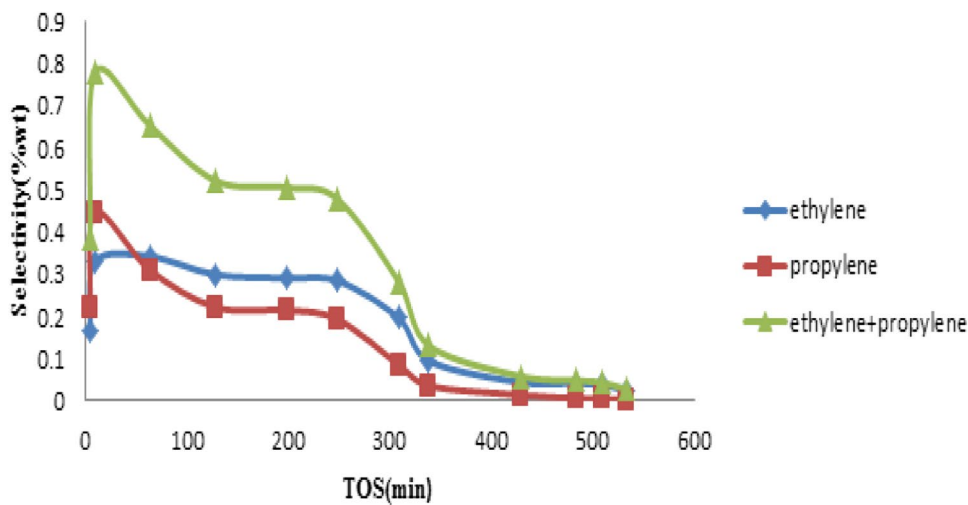


Fig. 13 Catalyst S8 reactor performance (synthesized at 210 °C for 24 h)

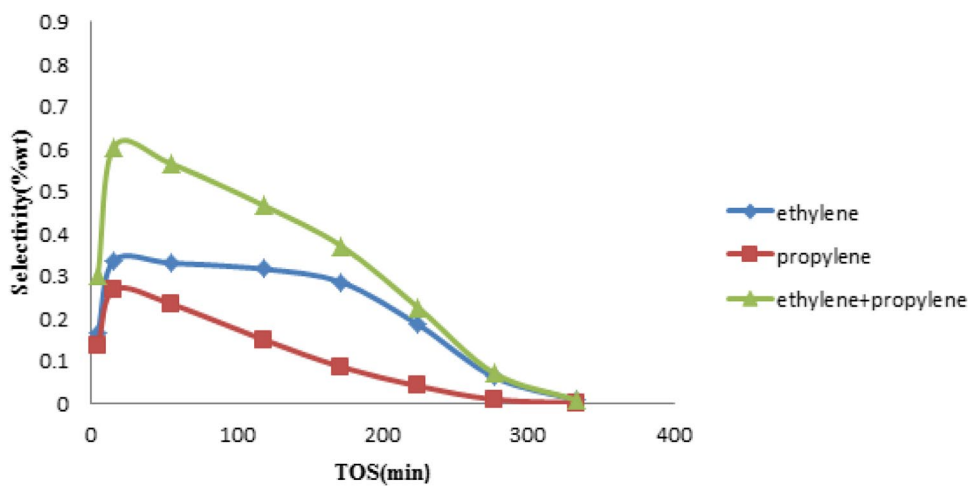


Fig. 14 Catalyst S9 reactor performance (synthesized at 210 °C for 36 h)

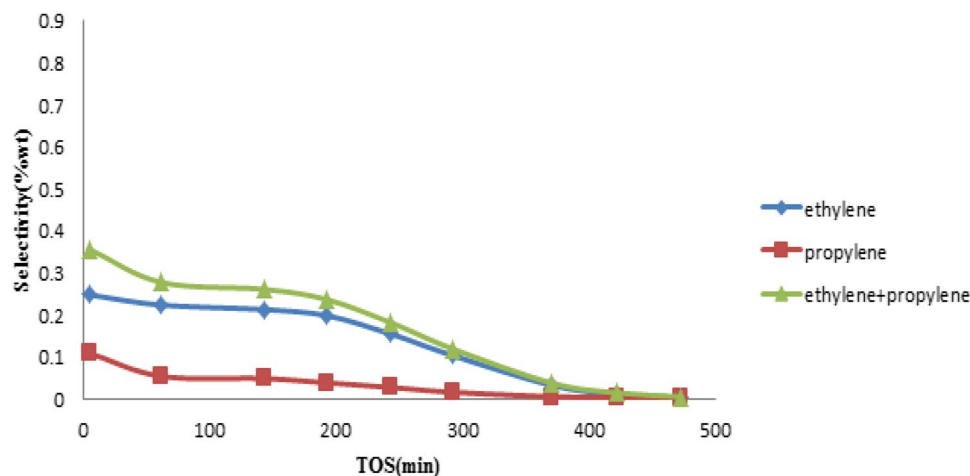


Table 5 The selectivity of light olefins for different samples

Samples	Selectivity C ₃ H ₅ (%)	Selectivity C ₂ H ₆ (%)
SAPO-34(S ₁)	32.00	34.50
SAPO-34(S ₂)	32.60	48.70
SAPO-34(S ₃)	31.80	43.50
SAPO-34(S ₄)	33.20	29.60
SAPO-34(S ₅)	33.60	24.80
SAPO-34(S ₆)	30.40	27.95
SAPO-34(S ₇)	33.10	44.90
SAPO-34(S ₈)	33.60	26.80
SAPO-34(S ₉)	24.70	10.85

time (15 min) is different from other S4, S5, S6, and S8 samples. However, due to the limitations of analyzing with a gas chromatograph and testing at regular intervals, this difference is less visible in the drawn charts, and in most catalysts after the second injection of gas products into the gas chromatography analysis machine., Selectivity increases significantly.

In the second stage, catalysts have the highest conversion to light olefins. During this time, methanol enters the active sites and the reaction is favored. Production of light olefins is high at this stage.

In the third step, where catalyst deactivation occurs, the smaller molecules block the cavities by secondary reactions and become larger coke molecules, preventing the methanol from penetrating the catalyst and preventing the reaction from continuing.

Sample S9 (synthesized at 210 °C and 36 h) Compared to other samples, it has a faster selectivity drop than olefins. This could be due to a large amount of amorphous phase (low crystallization percentage) and the presence of some SAPO-5 crystals in the composition. SAPO-5 with AFI structure and one-dimensional with large holes with

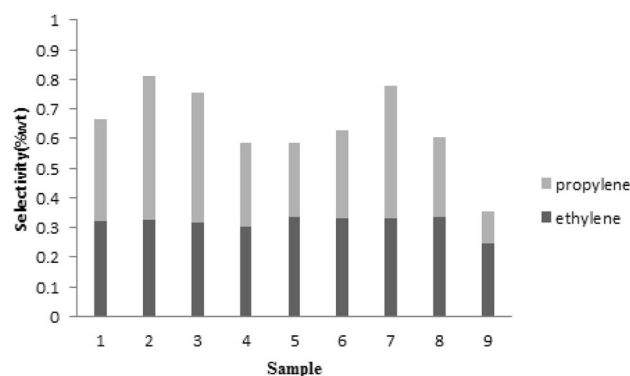


Fig. 15 Maximum selectivity diagram of light olefins for synthesized catalysts

dimensions 7.3°A × 7.3°A is which provides the right conditions for larger molecules to form. These large molecules, which can also be propylene and butylene, gradually with secondary reactions and creating heavier hydrocarbon species closes the holes And coking catalysts are and reduce catalyst lifetime. Due to all forms of selectivity, propylene drop is faster than ethylene. This is because the empty volume in the structure of the catalytic cavities decreases due to the formation of larger hydrocarbon species such as methylnaphthalene, phonation, and Pyrene. These species then act as organic centers (within the non-organic structure of SAPO-34), absorb methyl groups, and produce more ethylene instead of propylene. The selectivity values of all samples are reported in Table 5. As shown in Fig. 15, for samples S1, S2 and S3 synthesized at a constant temperature of 170 °C at different times of 12, 24, and 36 h, with the increased synthesis of each sample, was first increased and then decreased. The incremental trend of these three samples corresponds to the trend of their crystallinity percentage because with increase crystallinity percentage (low amorphous phase and incomplete structures in the sample),

Table 6 Catalytic performance results of SAPO-34 samples modified with different templates

Synthesis method	Crystallization temperature (° C)	Crystallization time (hr)	Molar ratios	Crystal size	Selectivity Ethylene (%)	Selectivity propylene (%)	Reference
Hydrothermal	200	12	AL ₂ O ₃ : P ₂ O ₅ : 0.6SiO ₂ : 1.5MOR: 0.5TEAOH:	Nano-Sized cubic aggregation 1 μm	45.6	36.2	[45]
Hydrothermal	200	24	AL ₂ O ₃ : P ₂ O ₅ : 0.25SiO ₂ : 1.8TEA: 0.2TEAOH:	1.4	49.6	37.6	[48]
microwave	180	1	AL ₂ O ₃ : 2P ₂ O ₅ : 0.6SiO ₂ : 4TEAOH: 140H ₂ O	20	42	39	[57]
Hydrothermal	4130	10,180	AL ₂ O ₃ : P ₂ O ₅ : 0.6SiO ₂ : 0.5TEAOH: 65H ₂ O	160	50.9	34.1	[59]

the selectivity increases. The trend for the samples (S9, S6, S3), (S6, S5, S4) and (S9, S8, S7) is also consistent with the crystallinity of the samples. For samples S7, S4, S1, which were synthesized at 12 h crystallization and different crystallization temperatures of 170, 190, and 210 °C. the process for selectivity was initially reduced by increasing the synthesis temperature to 190 °C, then the selectivity increased with increasing temperature to 210 °C, which is the opposite of the trend of crystal size, that is, with increasing synthesis temperature, the size of the crystals initially increased and then decreased. This can be explained by the fact that as the crystals grow larger, the penetration path lengths are also long in the cavities, and the products produced along the exit path of the cavity undergo secondary reactions, thereby reducing their selectivity [45]. However, the decreasing and then increasing selectivity trend for S2, S5, and S8 samples (samples synthesized at 24 h constant crystallization and different temperatures of 170, 190, and 210 °C) is also consistent with this logic and BET and TPD analysis of these samples. (Because of the higher the specific surface area and the acidity, the greater the benefit of producing light olefins), it can be interpreted [45]. Research on the effect of temperature and crystallization time on the SAPO-34 catalyst shows Most of the activities are related to the effect of these parameters on morphology and catalyst properties and except in a few cases, the catalyst function has not been studied in the MTO process. The results of the papers show Simultaneous changes in temperature and time can affect the structural and acidic properties of the SAPO-34 catalyst, resulting in

the production of light olefins in the MTO process. According to the table, the selectivity of ethylene and propylene is obtained in this study, although the size of the crystals was micro-scale, It is comparable to research whose nanoparticles have been nanoscale. Also, the catalyst synthesized in this study has a high selectivity compared to ethylene and can be used in research that aims to produce high ethylene. The comparison of our catalytic behavior in the MTO reaction with those SAPO-34 samples prepared with different soft templates by other researchers is reported in Table 6.

4 Conclusion

Sample S2 (synthesized at 170 °C and 24 h) with relatively small crystals size, high relative crystallinity percentage, highest surface area, and high acidic strength has the highest selectivity to light olefins, followed by S7 sample (synthesis). At 210 °C (12 h), with a slight difference, it provides the most selectivity for light olefins. Sample S9 (synthesized at 210 C and 36 h time) due to the high amorphous phase, low crystallinity percentage, and impure SAPO-5 phase compared to other catalysts show shorter lifetime and low selectivity. Sample S1 (synthesized at 170 C and 12 h) due to its small crystal size, high crystallinity, and medium acidity has the longest lifetime. According to the results of increasing temperature or crystallization time, due to the formation of the amorphous phase, it was not in favor of crystallinity and

was selected as the optimal catalyst for sample S2 catalyst operation.

Acknowledgements The authors gratefully a Department of Chemical Engineering, Arak Branch, Islamic Azad University, Arak, Iran and Young Researchers and Elite Club, Gachsaran Branch, Islamic Azad University, Gachsaran

Funding There is no funding to report for this submission.

Compliance with Ethical Standards

Conflict of interest The authors declare that they have no conflict of interest.

References

- Dubois DR, Obrzut DL, Liu J, Thundimadathil J, Adekanattu PM, Guin JA, Punnoose A, Seehra MS (2003) Conversion of methanol to olefins over cobalt-, manganese- and nickel-incorporated SAPO-34 molecular sieves. *Fuel Process Technol* 83(1–3):203–218
- Park JY, Lee YJ, Jun KW, Bae JW, Viswanadham N, Kim YH (2009) Direct conversion of synthesis gas to light olefins using dual bed reactor. *J Ind Eng Chem* 15(6):847–853
- Fatourehchi N, Sohrabi M, Royaei SJ, Mirarefin SM (2011) Preparation of SAPO-34 catalyst and presentation of a kinetic model for methanol to olefin process (MTO). *Chem Eng Res Des* 89(6):811–816
- <https://www.uop.com/mto-process-flow-scheme>, 2011.
- Alwahabi S (2003) Conversion of methanol to light olefins on SAPO-34 kinetic modeling and reactor design, PhD Thesis, Texas A&M University USA
- Jean L (2005) Effect of process parameters on methanol to olefins reactions over SAPO catalysts, Master's Thesis, Auburn University Alabama
- Dahl IM, Kolboe M (1994) On the reaction mechanism for hydrocarbon formation from methanol over SAPO-3. *J Catal* 149(1):458–464
- Dahl IM (1993) On the reaction mechanism for propene formation in the MTO reaction over SAPO-34. *Catal Lett* 20(3–4):329–336
- https://www.netl.doe.gov/technologies/coalpower/gasification/gasification/6-apps/6-5-2_coal-to-derivative.html, 2011
- Echevskii GV, Ione KG, Nosyreva GN, Litvak GS (1988) Effect of the temperature regime of methanol conversion to hydrocarbons on coking of zeolite catalysts and their regeneration. *Appl Catal* 43(1):85–89
- Chang CD, Lang WH, Smith RL (1979) The conversion of methanol and other O-compounds to hydrocarbons over zeolite catalysts: II. pressure effects. *J Catal* 56(2):169–173
- Comelli RA, Figoli NS (1991) Effect of pressure on the transformation of methanol into hydrocarbons on an amorphous silica-alumina. *Appl Catal* 73(2):185–194
- Liu L, Tobias RG, McLaughlin K, Anthony RG, (1984) Conversion of methanol to low molecular weight olefins with heterogeneous catalysts;" catalytic conversion of synthesis gas and alcohols to chemicals, R. G. Herman (Ed.), Plenum Press, New York, 323–360
- Marchi AJ, Froment GF (1991) Catalytic conversion of methanol to light alkenes on SAPO molecular sieves. *Appl Catal* 71(1):139
- Wu X, Anthony RG (2001) Effect of feed composition on methanol conversion to light olefins over SAPO-34. *J Catal* 218(1–2):241–250
- Park TY, Froment G (2001) Kinetic modeling of the methanol to olefins process. 2. Experimental results, model discrimination, and parameter estimation. *Ind Eng Chem Res* 40(20):4187–4196
- Froment GF, Dehertog WJH, Marchi AJ (1992) Zeolite catalysis in the conversion of methanol into olefins. *Catalysis* 9:1–64
- Chen JQ, Bozzano A, Glover B, Fuglerud T, Kvisle S (2005) Recent advancements in ethylene and propylene production using the UOP/Hydro MTO process. *Catal Today* 106(1–4):103–107
- Pastore HO, Coluccia S, Marchese L (2005) Porous aluminophosphates: from molecular sieves to designed acid catalysts. *First publ online Rev Adv* 35:351–395
- Guangyu L, Peng T, Zhongmin L (2012) Synthesis of SAPO-34 molecular sieves templated with diethylamine and their properties compared with other templates. *Chin J Catal* 33(1):174–182
- Xu R, Pang W, Yu J, Huo Q, Chen J, (2006) Chemistry of zeolites and related porous materials: synthesis and structure: synthesis of zeolites, Chapter 3, 52
- Salmasi M, Fatemi S, Najafabadi AT (2011) Improvement of light olefins selectivity and catalyst lifetime in MTO reaction; using Ni and Mg-modified SAPO-34 synthesized by combination of two templates. *J Ind Eng Chem* 17(4):755–761
- Inui T, Kang M (1997) Reliable procedure for the synthesis of Ni-SAPO-34 as highly selective catalyst for methanol to ethylene conversion. *Appl Catal A* 164(1–2):211–223
- Djeugoue MA, Prakash AM, Kevan L (1999) Electron spin resonance and electron spin-echo modulation studies of synthesized NiAPSO-34 molecular sieve and comparison with ion-exchanged NiH-SAPO-34 molecular sieve. *J Phys Chem B* 103(5):804–811
- Cola PLD, Glaser R, Weitkamp J (2006) Non-oxidative propane dehydrogenation over Pt–Zn-containing zeolites. *Appl Catal A* 306(7):85–97
- Hochtl M, Jentys A, Vinek H (2001) Isomerization of 1-pentene over SAPO, CoAPO (AEL, AFI) molecular sieves and HZSM-5. *Appl Catal A* 207(1–2):397–405
- Wilson S, Barger P (1999) The characteristics of SAPO-34 which influence the conversion of methanol to light olefins. *Microporous Mesoporous Mater* 29(1–2):117–126
- Zibrowius B, Löffler E, Hunger M (1992) Multinuclear MAS n. m. r. and I. r. spectroscopic study of silicon incorporation into SAPO-5, SAPO-31, and SAPO-34 molecular sieves. *Zeolites* 12(2):167–174
- Zubkov SA, Kustoy LM, Kazansky VB (1991) Investigation of hydroxyl groups in crystalline silicoaluminophosphate SAPO-34 by diffuse reflectance infrared spectroscopy. *J Chem Soc, Faraday Trans* 87(87):897–900
- Liu G, Tian P, Li J, Zhang D, Zhou F, Liu Z (2008) Synthesis, characterization and catalytic properties of SAPO-34 synthesized using diethylamine as a template. *Microporous Mesoporous Mater* 111(1–3):143–149
- Dahl IM, Mostad H, Akporiaye D, Wendelbo R (1999) Structural and chemical influences on the MTO reaction: a comparison of chabazite and SAPO-34 as MTO catalysts. *Microporous Mesoporous Mater* 29(1–2):185–190
- Sastre G, Lewis DW, Catlow CRA (1997) Modeling of silicon substitution in SAPO-5 and SAPO-34 molecular sieves. *J Phys Chem B* 101(27):5252–5262
- Hajjashrafi T, Kharat AN (2013) Study of preparation methods and their effect on the morphology and texture of SAPO-34 for the methanol to olefin reaction. *React Kinet Mech Catal* 108(2):417–432

34. Emrani P, Fatemi Sh, Talesh SA (2011) Effect of synthesis parameters on phase purity, crystallinity and particle size of SAPO-34. *Iran J Chem Chem Eng* 30(4):29–36
35. Tan J, Liu Z, Bao X, Liu X, Han X, He Ch, Zhai R (2002) Crystallization and Si incorporation mechanisms of SAPO-34. *Microporous Mesoporous Mater* 53(1–3):97–108
36. Izadbakhsh A, Farhadi F, Khorasheh F, Sahebdehfar S, Asadi M, Feng YZ (2009) Effect of SAPO-34's composition on its physico-chemical properties and deactivation in MTO process. *Appl Catal A* 364(1–2):48–56
37. Shen W, Li X, Wei Y, Tian P, Deng F, Han X, Bao X (2012) A study of the acidity of SAPO-34 by solid-state NMR spectroscopy. *Microporous Mesoporous Mater* 158:19–25
38. Wang J, Yu T, Wang X, Qi G, Xue J, Shen M, Li W (2012) The influence of silicon on the catalytic properties of Cu/SAPO-34 for NO_x reduction by ammonia-SCR. *Appl Catal B* 127:137–147
39. Izadbakhsh A, Farhadi F, Khorasheh F, Sahebdehfar S, Asadi M, Yan ZF (2009) Key parameters in hydrothermal synthesis and characterization of low silicon content SAPO-34 molecular sieve. *Microporous Mesoporous Mater* 126(1–2):1–7
40. Xu L, Du A, Wei Y, Wang Y, Yu Z, He Y, Zhang X, Liu Z (2008) Synthesis of SAPO-34 with only Si(4Al) species: effect of Si contents on Si incorporation mechanism and Si coordination environment of SAPO-34. *Microporous Mesoporous Mater* 115(3):332–337
41. Heyden HV, Mintova S, Bein T (2008) Nanosized SAPO-34 synthesized from colloidal solutions. *Chem Mater* (ACS Publications) 20(9):2956–2963
42. Hirota Y, Murata K, Tanaka S, Nishiyama N, Egashira Y, Ueyama K (2010) Dry gel conversion synthesis of SAPO-34 nanocrystals. *Mater Chem Phys* 123(2–3):507–509
43. Lin S, Li J, Sharma RP, Yu J, Xu R (2010) Fabrication of SAPO-34 crystals with different morphologies by microwave heating. *Top Catal* 53(19–20):1304–1310
44. Popova M, Minchev Ch, Kanazirev V (1998) Methanol conversion to light alkenes over SAPO-34 molecular sieves synthesized using various sources of silicon and aluminium. *Appl Catal A* 169(2):227–235
45. Lee YJ, Baek SC, Jun KW (2007) Methanol conversion on SAPO-34 catalysts prepared by mixed template method. *Appl Catal A* 329:130–136
46. Shirazi L, Gangji E, Taheri Z (2011) The Effect of H-SAPO-34 Template Type on Conversion of Methanol to Light Olefins, *J Oil Res*, doi: <https://doi.org/10.22078/pr.2013.89>
47. Nishiyama N, Kawaguchi M, Hirota Y, Vu DV, Egashira Y, Ueyama K (2009) Size control of SAPO-34 crystals and their catalyst lifetime in the methanol-to-olefin reaction. *Appl Catal A* 362(1–2):193–199
48. Wang P, Lv A, Hu J, Xu J, Lu G (2012) The synthesis of SAPO-34 with mixed template and its catalytic performance for methanol to olefins reaction. *Microporous Mesoporous Mater* 152:178–184
49. Hajfarajollah H, Askari S, Halladj R (2014) Effects of micro and nano-sized SAPO-34 and SAPO-5 catalysts on the conversion of methanol to light olefins. *Reac Kinet Mech Cat* 111(723–736):2014
50. Alvaro-Muñoz T, Marquez-Alvarez C, Sastre E (2014) Aluminium chloride: a new aluminium source to prepare SAPO-34 catalysts with enhanced stability in the MTO process. *General, Appl Catal A: General* 472:72–79
51. Dargahia M, Kazemianb H, Soltanieh M, Rohanib S, Hosseinpour M (2011) Rapid high-temperature synthesis of SAPO-34 nanoparticles. *Particuology* 9(5):452–457
52. Lee KY, Chae H-J, Jeong S-Y, Seo G (2009) Effect of crystallite size of SAPO-34 catalysts on their induction period and deactivation in methanol-to-olefin reactions. *Appl Catal A* 369(1–2):60–66
53. Guangyu L, Peng T, Zhongmin L (2012) Synthesis of SAPO-34 molecular sieves templated with diethylamine and their properties compared with other templates. *Chin J Catal* 33(1):74–182
54. Lei W, Ziyu L, Lin X, Minghuang Q, Xu L, Haojia Z, Yuhua S (2013) Effect of SAPO-34 molecular sieve morphology on methanol to olefins performance. *Chin J Catal* 34(7):1348–1356
55. Valizadeh B, Askari S, Halladj R, Haghmoradi A (2014) Synthesis and reactivity in inorganic metal-organic, and nano-metal chemistry. *Synth React Inorg Metal-Org Nano-Metal Chem* 44(1):79–83
56. Alvaro-Muñoz T, Marquez-Alvarez C, Sastre E (2012) Use of different templates on SAPO-34 synthesis: effect on the acidity and catalytic activity in the MTO reaction". *Catal Today* 179(2012):27–34
57. Yang G, Wei Y, Xu S, Chen J, Li J, Liu Zh, Yu J, Xu R (2013) Nanosize-enhanced lifetime of SAPO-34 catalysts in methanol-to-olefin reactions. *J Phys Chem C* 117:8214–8222
58. Topuz B, Oral E, Kalipcilar H (2013) Low temperature synthesis of SAPO-34 in a recirculating-flow system. *J Porous Mater* 20(1491–1500):2013
59. Wang P, Yang D, Hub J, Xu J, Lu G (2013) Synthesis of SAPO-34 with small and tunable crystallite size by two-step hydrothermal crystallization and its catalytic performance for MTO reaction. *Catal Today* 212(2013):62.e1–62.e8
60. Lok BM, Messina CA, Patton RL, Gajek RT, Cannan TR, Flanigen EM (1984) Crystalline silicaluminophosphates, US Patent 4,440,871 B01J, Union Carbide Corporation, Danbury, Conn
61. Girnus I, Jancke K, Vetter R, Richter-Mendau J, Caro J (1995) Large ALPO₄-5 crystals by microwave heating. *Zeolites* 15(1):33–39
62. Demuth D, Stucky GD, Unger KK, Schuth F (1995) Synthesis of large optically clear silicoaluminophosphate crystals with AFI structure. *Microporous Mater* 3(4–5):473–487
63. Coluccia S, Marchese L, Martra G (1999) Characterisation of microporous and mesoporous materials by the adsorption of molecular probes: FTIR and UV–Vis studies. *Microporous Mesoporous Mater* 30(1):43
64. Wilson ST (2009) Synthesis of SAPO-34 with essentially pure CHA framework, US Patent 7578987 B2 Uop Llc.
65. Casady JB, Johnson RW (1996) Status of silicon carbide (SiC) as a wide-bandgap semiconductor for high-temperature applications: a review. *Solid-State Electron* 39(10):1409–1422
66. Zubko Y SA, Kustoy LM, Kazansky VB (1991) Investigation of hydroxyl groups in crystalline silicoaluminophosphate SAPO-34 by diffuse reflectance infrared spectroscopy. *J Chem Soc Faraday Trans* 87(1991):897–900
67. Utchariyajit K, Wongkasemjit S (2010) Effect of synthesis parameters on mesoporous SAPO-5 with AFI-type formation via microwave radiation using alumatrane and silatrane precursors. *Microporous Mesoporous Mater* 135(1–3):116–123
68. Wei YX, Zhang DZ, He YL, Xu L, Yang Y, Su BL, Liu ZM (2007) Catalytic performance of chloromethane transformation for light olefins production over SAPO-34 with different Si content. *Catal Lett* 114(1–2):30
69. Mirza Kh, Ghadiri M, Haghghi M, Afghan A (2018) Hydrothermal synthesis of modified Fe, Ag and K-SAPO-34 nanostructured catalysts used in methanol conversion to light olefins. *Microporous Mesoporous Mater* 260:155–165
70. Hang Y, Qu M, Ukkusuri S (2011) Optimizing the design of a solar cooling system using central composite design techniques. *Energy Build* 43:988–994
71. Kianfar E, Salimi M, Pirouzfard V, Koohestani B (2018) Synthesis and modification of Zeolite ZSM-5 catalyst with solutions of calcium carbonate (CaCO₃) and sodium carbonate (Na₂CO₃) for methanol to gasoline conversion. *Int J Chem React Eng* 16(7):1–7

72. Kianfar E, Salimi M, Hajimirzaee S, Koohestani B (2019) Methanol to gasoline conversion over CuO/ZSM-5 catalyst synthesized using sonochemistry method. *Int J Chem React Eng* 17(2):1–10
73. Kianfar E (2018) Synthesis and characterization of AlPO₄/ZSM-5 catalyst for methanol conversion to dimethylether. *Russ J Appl Chem* 91(10):1710–1720
74. Kianfar E (2019) Recent advances in synthesized, properties, applications of Nano- zeolites. *J Sol-Gel Sci Technol* 91(2):415–429
75. Kianfar E, Salimi M, Pirouzfard V, Koohestani B (2018) Synthesis of modified catalyst and stabilization of CuO/NH₄-ZSM-5 for conversion of methanol to gasoline. *Int J Appl Ceram Technol* 15(3):734–741
76. Kianfar E (2019) Comparison and assessment of Zeolite Catalysts performance Dimethyl ether and light olefins production through methanol: A review. *Rev Inorg Chem* 39(3):157–177
77. Kianfar E (2019) Ethylene to propylene over zeolite ZSM-5: Improved catalyst performance by treatment with CuO. *Russ J Appl Chem* 92(7):933–939
78. Kianfar E (2019) Ethylene to propylene Conversion over Ni-W/ZSM-5 Catalyst Synthesize. *Russ J Appl Chem* 92(8):1094–1101
79. E Kianfar (2019) *Microchem J* <https://doi.org/10.1016/j.microc.2020.104822>.
80. Kianfar E, Mahmoud Salimi M, A Review on the Production of Light Olefins from Hydrocarbons Cracking and Methanol Conversion: In book: *Advances in Chemistry Research*, Volume 59: Edition: James C. Taylor Chapter: 1 :Publisher: Nova Science Publishers, Inc., NY, USA.
81. Kianfar E, Razavi A, Zeolite catalyst based selective for the process MTG: A review: In book: *Zeolites: Advances in Research and Applications*, Edition: Annett Mahler Chapter: 8: Publisher: Nova Science Publishers, Inc., NY, USA
82. Kianfar E, Zeolites: Properties, Applications, Modification and Selectivity: In book: *Zeolites: Advances in Research and Applications*, Edition: Annett Mahler Chapter: 1: Publisher: Nova Science Publishers, Inc., NY, USA
83. Kianfar E, Azimikia R, Faghih SM (2020) Simple and strong dative attachment of α -diimine nickel (ii) catalysts on supports for ethylene polymerization with controlled morphology. *Catal Lett.* <https://doi.org/10.1007/s10562-020-03116-z>
84. Zhao X, Li D, Yang B, Ma C, Zhu Y, Chen H (2014) Feature selection based on improved ant colony optimization for online detection of foreign fiber in cotton. *Appl Soft Comp* 24:585–596
85. Wang M, Chen H (2020) Chaotic multi-swarm whale optimizer boosted support vector machine for medical diagnosis. *Appl Soft Comp* 88:105946
86. Zhao X et al (2019) Chaos enhanced grey wolf optimization wrapped ELM for diagnosis of paraquat-poisoned patients. *Comput Biol Chem* 78:481–490
87. Xu X, Chen H-L (2014) Adaptive computational chemotaxis based on field in bacterial foraging optimization. *Soft Comput* 18(4):797–807
88. Shen L et al (2016) Evolving support vector machines using fruit fly optimization for medical data classification. *Knowl-Based Syst* 96:61–75
89. Wang M et al (2017) Toward an optimal kernel extreme learning machine using a chaotic moth-flame optimization strategy with applications in medical diagnoses. *Neurocomputing* 267:69–84
90. Xu Y, Chen H, Luo J, Zhang Q, Jiao S, Zhang X (2019) Enhanced Moth-flame optimizer with mutation strategy for global optimization. *Inf Sci* 492:181–203
91. Chen H, Zhang Q, Luo J, Xu Y, Zhang X (2020) An enhanced bacterial foraging optimization and its application for training kernel extreme learning machine. *Appl Soft Comp* 86:105884
92. Zhang, Xianwen, Dynamic information of the time-dependent to bullian biomolecular structure using a high-accuracy size-dependent theory
93. Najaafi N, Dynamic instability responses of the substructure living biological cells in the cytoplasm environment using stress-strain size-dependent theory, 10.1080/07391102.2020.1751297
94. Hossein Moayedi, Weld orientation effects on the formability of tailor welded thin steel sheets. <https://doi.org/10.1016/j.tws.2020.106669>
95. Ghabussi A, Free vibration analysis of an electro-elastic GPLRC cylindrical shell surrounded by viscoelastic foundation using modified length-couple stress parameter. <https://doi.org/10.1080/15397734.2019.1705166>
96. Ghabussi A, Improving seismic performance of portal frame structures with steel curved dampers. <https://doi.org/10.1016/j.istruc.2019.12.025>
97. Shariati A, Extremely large oscillation and nonlinear frequency of a multi-scale hybrid disk resting on nonlinear elastic foundation. <https://doi.org/10.1016/j.tws.2020.106840>

Publisher's Note Springer Nature remains neutral with regard to jurisdictional claims in published maps and institutional affiliations.

Affiliations

Haiyan Liu¹ · Ehsan Kianfar^{2,3}

✉ Haiyan Liu
zjliuhaiyan@126.com

✉ Ehsan Kianfar
e-kianfar94@iau-arak.ac.ir; ehsan_kianfar2010@yahoo.com

¹ Yiwu Industrial & Commercial College, Zhejiang 322000, China

² Department of Chemical Engineering, Arak Branch, Islamic Azad University, Arak, Iran

³ Young Researchers and Elite Club, Gachsaran Branch, Islamic Azad University, Gachsaran, Iran